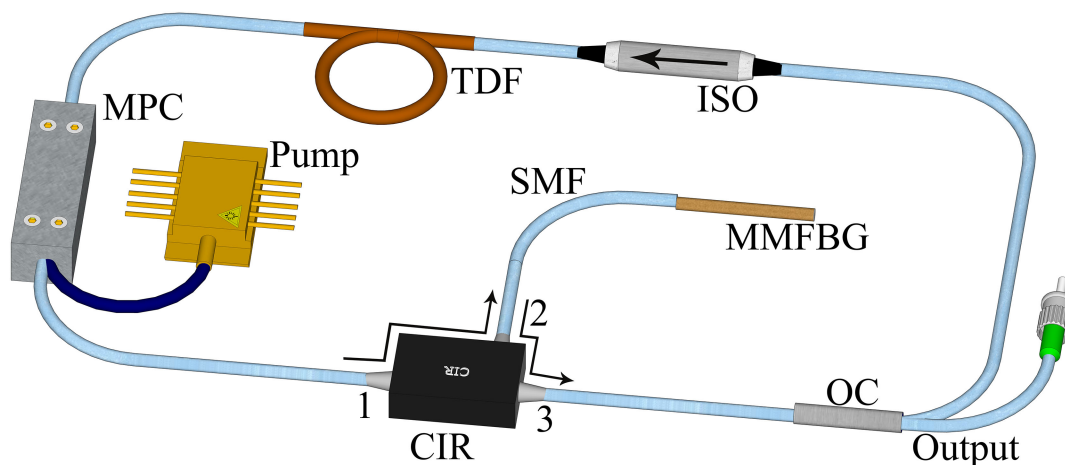


Twelve-Wavelength-Switchable Thulium-Doped Fiber Laser With a Multimode Fiber Bragg Grating






Volume 13, Number 3, June 2021

Qi Qin
Fengping Yan
Yan Liu
Zhenchen Cui
Dan Cheng
Chenhao Yu
Youchao Jiang
Yuping Suo
Hong Zhou
Ting Feng



DOI: 10.1109/JPHOT.2021.3084929

Twelve-Wavelength-Switchable Thulium-Doped Fiber Laser With a Multimode Fiber Bragg Grating

Qi Qin ¹, Fengping Yan ¹, Yan Liu ¹, Zhenchen Cui,¹
Dan Cheng,¹ Chenhao Yu,¹ Youchao Jiang ¹, Yuping Suo,²
Hong Zhou,³ and Ting Feng ⁴

¹Key Laboratory of All Optical Network and Advanced Telecommunication Network, Ministry of Education, Institute of Lightwave Technology, Beijing Jiaotong University, Beijing 100044, China

²Shanxi Provincial People's Hospital, Shanxi Medical University, Taiyuan 030012, China

³Department of Electronics Information and Communication Engineering, Osaka Institute of Technology, Asahi-ku, Osaka 535-8585, Japan

⁴Photonics Information Innovation Center, Hebei Provincial Center for Optical Sensing Innovations, College of Physics Science & Technology, Hebei University, Baoding 071002, China

DOI:10.1109/JPHOT.2021.3084929

This work is licensed under a Creative Commons Attribution 4.0 License. For more information, see <https://creativecommons.org/licenses/by/4.0/>

Manuscript received April 18, 2021; revised May 24, 2021; accepted May 26, 2021. Date of publication May 31, 2021; date of current version June 14, 2021. This work was supported in part by the Fundamental Research Funds for the Central Universities under Grant 2020YJS009, and in part by the National Natural Science Foundation of China under Grants 61827818, 61620106014, 61775128, 61975009, 61975049, and 62005013. Corresponding authors: Fengping Yan; Yan Liu (e-mail: fpyan@bjtu.edu.cn; yanliu@bjtu.edu.cn).

Abstract: In this article, a precisely controlled, switchable thulium-doped fiber laser (TDFL) with high optical signal-to-noise ratio (OSNR) is proposed and demonstrated. A home-made multimode fiber Bragg grating (MMFBG) with multireflection peaks was used as an optical filter to select the desired lasing channel. Using a manually controlled fusion splicer, the axial misalignment was applied between the single mode fiber and the MMFBG to switch the output wavelength. In the experiment, the number of switchable lasing lines was up to 12, and the fluctuation of the center wavelength and output power was less than 0.03 nm and 0.67 dB, respectively. A maximum slope efficiency of 1.3% was obtained when the axial misalignment was 0 μm , and the OSNR was higher than 65 dB. In addition, the proposed fiber laser was used as an optical fiber laser sensor to quantify the strain applied on the MMFBG, and a sensitivity of 1.16 pm/ μe was obtained.

Index Terms: Multimode fiber Bragg grating, thulium-doped fiber laser, optical fiber laser sensor.

1. Introduction

The thulium-doped fiber laser (TDFL) has attracted widespread interest due to the favorable characteristics of thulium-doped fiber (TDF). The wide lasing range (1700–2100 nm) [1] of TDF emitting at a 2 μm wavelength band makes the TDFL a potential light source in optical communication systems [2]–[4]. The characteristic of being readily absorbed by certain gas molecules facilitates the application of the TDFL in sensing gases, such as hydrocarbon gas [5] and CO₂ [6]. In addition, the lasing wavelength at this waveband can be highly absorbed by water, which leads

to substantial heating in small areas of biological tissue. Thus, the TDFL is well suited for cutting and vaporizing biological tissue [7], [8]. Furthermore, the TDFL has wide applications, such as in material processing [9], coherent Doppler lidar [10] and pump source in generating Mid-Infrared Super Continuum [11]. Thus, the TDFL is currently in great demand and needs to be further developed.

To date, various TDFLs have been proposed, including the TDFL with switchable output [12], [13], TDFL with single-longitudinal-mode operation [14], [15], mode-locked TDFL [16], [17] and high power TDFL [18]. The TDFL with switchable output is extensively used in optical fiber sensing and wavelength routing networks due to its flexible lasing performance. To obtain a switchable output, the wavelength selective component, including an acousto-optic tunable bandpass filter [19], digital micromirror array [20], Fabry-Perot (F-P) filter [21], Sagnac loop mirror [22], Mach-Zehnder interferometer [23], mode interference-based filter [24], tapered fiber [25] and fiber Bragg grating (FBG) [26], should be used. As a result of their good compatibility, narrow bandwidth, simple structure and small size, FBGs are widely used in TDFLs to obtain a switchable output. In 2013, W. Peng *et al.* proposed a linear cavity-based TDFL with a switchable single-wavelength output using two polarization-maintaining FBGs (PM-FBGs), in which a two switchable single-wavelength output with an orthogonal polarization state was obtained [26]. In 2014, six uniform FBGs were concatenated to form an FBG array, based on which six switchable lasing wavelengths were achieved in the 2 μm region [27]. S. Liu *et al.* built a TDFL with a two switchable single-wavelength output by combining a PM-FBG and a PM F-P filter, in which the optical signal-to-noise ratio (OSNR) of the single-wavelength operation can reach 60 dB [28]. More recently, based on a PM sampled fiber Bragg grating, a six-wavelength switchable output was obtained [14]. Importantly, the number of switchable output was less than six in the previous reports. The multimode fiber Bragg grating (MMFBG) with multireflection peaks, which has received widespread attention is a possible good candidate to further increase the number of switchable single-wavelength output [29]–[31].

The mechanism to obtain the switchable output is mainly based on adjusting the manually controlled polarization controller (PC) [14], [26], [28], which is always random and cannot be accurately controlled, or based on balancing the gain and loss in the cavity by multi-tubular mounts [27], which complicates the structure of the fiber laser. With an MMFBG, the reflection spectrum varies with the mode excitation conditions, which may result in more accurate and simpler output control.

In this study, an MMFBG based on a multimode fiber (MMF) with a core diameter of 62.5 μm is fabricated and tested. Then, with the home-made MMFBG, a TDFL with twelve-switchable output wavelengths is constructed. The manuscript is organized as follows. In section 2, the fabrication method of the MMFBG was described, and the characterization of polarization dependence and the reflection spectra under different launching conditions were discussed. Based on the analysis, a TDFL with a switchable single-wavelength output was constructed in section 3. In section 4, the performance of the fiber laser with respect to switchable output, stability and lasing efficiency was studied, and the potential application of a fiber laser sensor to measure the strain was demonstrated using the proposed fiber laser.

2. Fabrication and Testing of the MMFBG

The MMFBG was fabricated using the phase mask method [14] with a 248-nm KrF excimer laser. Different from the previous work [14], the grating was inscribed on a section of commercial graded-index multimode fiber (Nufern GI-62.5/125-S; Nufern Inc., Granby, CT, USA) with numerical aperture of 0.275, which was hydrogen-loaded for 14 days before the grating was inscribed, and the core/cladding diameter was 62.5/125 μm . The period and length of the uniform phase mask was 1347.3 nm and 2 cm, respectively. In the process of manufacturing, the peak power, repetition rate and scanning speed of the excimer laser were 60 mJ, 20 Hz and 0.05 mm/s, respectively.

Due to the large core diameter of the MMF, the ultraviolet writing may be nonuniform over the cross section of the MMF. Thus, it is necessary to measure the polarization dependence of the MMFBG. The experimental setup to measure the polarization dependence is shown in Fig. 1(a).

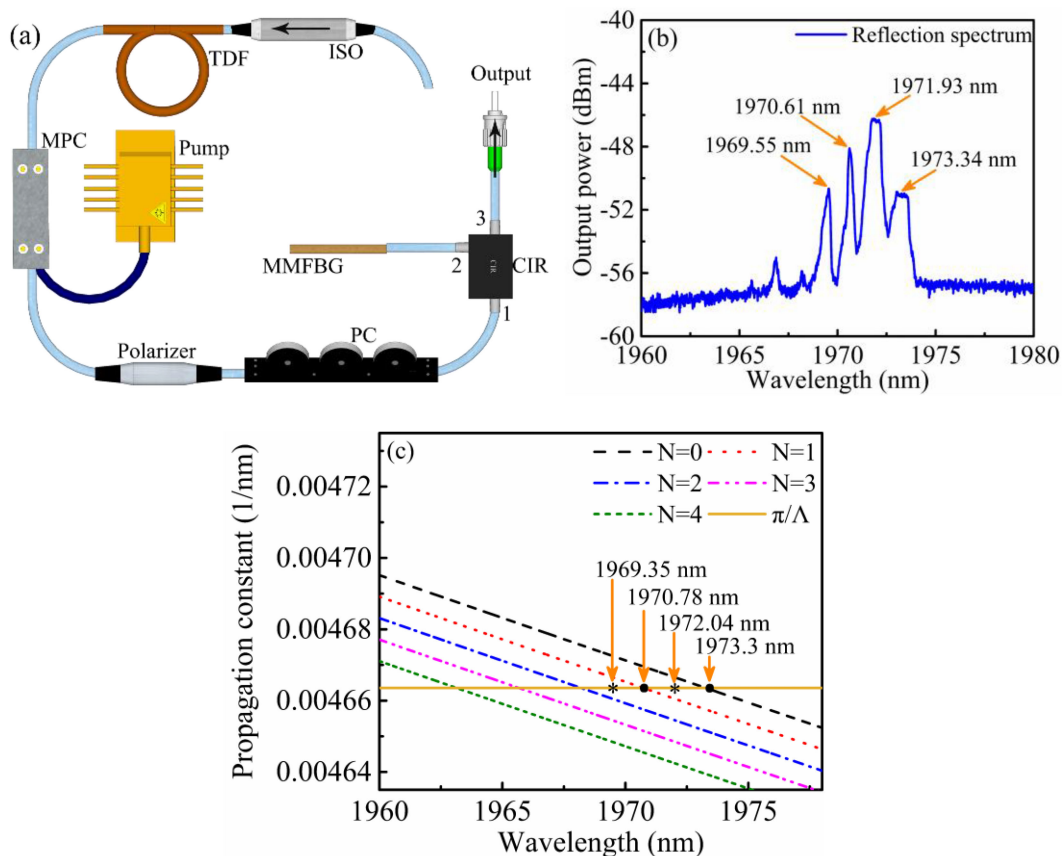


Fig. 1. (a) Measurement of the polarization dependence of the MMFBG, (b) a typical reflection spectrum of the MMFBG, (c) mode diagram of a Bragg grating in graded-index MMF. ISO: isolator, TDF: thulium-doped fiber, MPC: multimode pump combiner, PC: polarization controller, CIR: circulator, MMFBG: multimode fiber Bragg grating.

In the experiment, the pigtail of port 2 of the circulator (CIR) and the MMFBG are located closely together at a large axial misalignment using the FSU 975 fiber fusion splicer (Ericsson, Stockholm, Sweden). The axial misalignment between the single mode fiber and the multimode fiber induces the optical loss. If the pump power was too small, the reflection spectrum of the multimode fiber Bragg grating (MMFBG) cannot be observed with large axial misalignment. If the pump power was too high, the elements adopted in the experiment may suffer from damage. Thus, a moderate pump power of 4.21 W was used to test the characteristic of the MMFBG. With a pump power of 4.21 W injected into the TDF (SM-TDF-10P/130-M) by a multimode pump combiner (MPC, LightComm Technology, Co. Ltd., Shenzhen, China.), the amplified spontaneous emission (ASE) was generated, and then it was converted into linearly polarized emission by the polarizer. The state of polarization (SOP) was further adjusted by the three-loop PC. Then, the ASE with different SOPs was reflected by the MMFBG and captured by the optical spectrum analyzer (OSA) through port 3 of the CIR. Noted that, if the PC is placed before the polarizer, the polarizer was injected by ASE with different SOPs when the PC was tuned. However, the polarizer only allows a certain SOP to pass through. Thus, the intensity of the ASE output from the polarizer varied and the SOP remained unchanged. To measure the polarization dependence of the MMFBG, the ASE with different SOPs should be injected into the MMFBG. Thus, the PC was placed after the polarizer. A typical reflection spectrum is shown in Fig. 1(b) exhibiting four main reflection peaks. When the PC was tuned, the reflection spectrum remained unchanged. Thus, the home-made MMFBG is

polarization independent, which means that when it is applied in the TDFL, the switchable output cannot be obtained by tuning the PC.

To specify the locations of the reflection peaks, the phase matching condition is analysed [32], [33]. The phase matching condition of an FBG can be expressed as:

$$\beta_1 - \beta_2 = 2\pi/\Lambda \quad (1)$$

where β_1 and β_2 is the propagation constant of the forward and backward mode, respectively; Λ (673.65 nm) is the period of the Bragg grating. Considering that only the fundamental mode exists, the phase matching condition can be simplified as: $\beta = \pi/\Lambda$. The reflection peak appears once the phase matching condition is satisfied. In the graded-index MMF, the number of transmission modes can be calculated by:

$$M = \frac{1}{2}a^2k_0^2n_1^2\Delta \quad (2)$$

where a is core radius of the MMF, k_0 represents the wave number, n_1 is the axial refractive index of the core and $\Delta \approx (n_1 - n_2)/n_1$ denotes the relative refractive index difference. In this article, the refractive index of the core n_1 is 1.4665 and the number of modes M is ~ 187 at 1970 nm. However, most of the modes have almost the same propagation constant, which can be classified into the same principal mode. The propagation constant for the N_{th} principal mode can be expressed as:

$$\beta_{th} = \frac{2\pi}{\lambda}n_1\sqrt{1 - 4\Delta\frac{N+1}{V}} \quad (3)$$

where V represents the normalized frequency: $V = 2\pi aNA/\lambda$; N is the mode number. NA is the numerical aperture: $NA = \sqrt{n_1^2 - n_2^2}$, and n_2 is the refractive index of cladding.

The calculated propagation constants are shown in Fig. 1(c) and the parameters of the MMF are: $NA = 0.275$, $a = 31.25 \mu\text{m}$. The black solid dots correspond to the reflection wavelengths due to the coupling of the same mode, and the black asterisks indicate the Bragg wavelengths generated by the adjacent mode coupling. The calculated first four Bragg wavelengths are 1973.3, 1972.04, 1970.78 and 1969.35 nm, which are in accordance with the reflection wavelengths obtained in the experiment within a certain acceptable error range.

Importantly, when the single mode fiber (SMF) was connected with the MMF, the axial misalignment greatly influenced the excited modes in the MMF. Thus, with different mode excitation conditions, the MMFBG shows different reflection spectra. The characterization of the reflection spectrum under different axial misalignment condition is shown in Fig. 2(a). Due to the polarization independence, during the measurement of MMFBG, the ASE was injected directly into port 1 of the CIR when the pump power was 4.21 W. Then, the MMFBG was illuminated by the ASE through port 2 of the circulator with axial misalignment achieved by the manually controlled fusion splicer. The reflected spectrum was monitored by the OSA through port 3 of the circulator.

The relative reflection spectrum, which was obtained by subtracting the ASE spectrum from the reflection spectrum of the MMFBG, is displayed in Fig. 2(b). The images illustrating different launching conditions captured from the screen of the fusion splicer are inserted into the left-bottom of the sub-figures in Fig. 2(b). The value of axial misalignment (offset value) is calculated by the proportion of the cladding diameter and the lateral offset between the two fibers. With the increase of axial misalignment, the intensity of peak 1 varied, as shown in the inset of the first column of Fig. 2(b). Also, with the decrease of the intensity of peak 1, the value of peak 2 increases gradually. When the axial misalignment is ~ 7.92 nm, the intensity of peak 2 is higher than that of peak 1. Therefore, with the increase of axial misalignment, the peak with higher intensity appears in different wavelength and accordingly the different output wavelength could be obtained.

3. Experimental Setup of the TDFL

The experimental setup of the proposed TDFL is shown in Fig. 3. The double clad TDF (SM-TDF-10P/130-M; Nufern Inc.) had a peak cladding absorption at 793 nm of 4.5 dB/m and a core/cladding

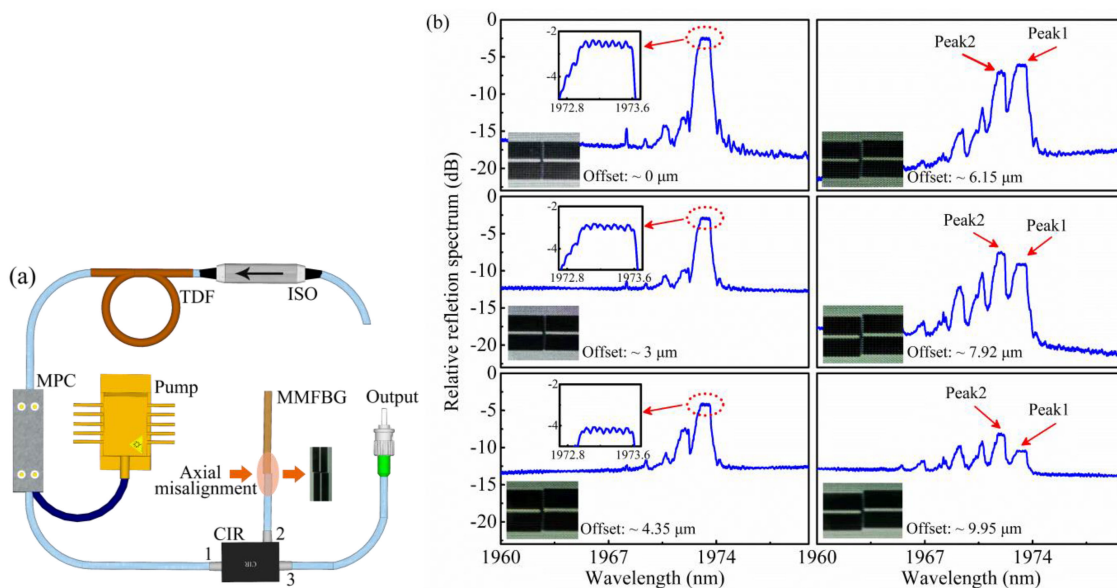


Fig. 2. (a) Experimental setup for measuring the reflection spectrum of the MMFBG, (b) relative reflection spectrum under different axial misalignment. ISO: isolator, TDF: thulium-doped fiber, MPC: multimode pump combiner, CIR: circulator, MMFBG: multimode fiber Bragg grating.

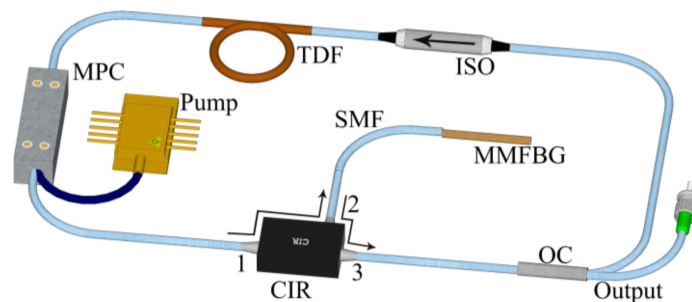


Fig. 3. Experimental setup of the proposed TDFL. ISO: isolator, TDF: thulium-doped fiber, MPC: multimode pump combiner, CIR: circulator, MMFBG: multimode fiber Bragg grating, OC: optical coupler, SMF: single mode fiber.

numerical aperture of 0.15/0.45. A 793-nm laser diode (BWT Beijing Ltd., Beijing, China) with a maximum output power of 12 W was used as the pump source, and the pump signal was injected into the TDF through the $(2+1)\times 1$ MPC. The polarization insensitive SMF isolator was inserted into the cavity to force the anti-clockwise transmission. The ASE went through port 1 and port 2 of the polarization insensitive CIR in turn, and reflected by the MMFBG. The pigtail (SMF-28e) of port 2 and the MMFBG were closely located by using the fusion splicer in manually controlled mode. The reflected light went through port 3 of the CIR and was coupled out by the 10% port of the optical coupler. Another output port (90% port) of the OC was connected with the ISO to construct the ring cavity. The output spectrum was recorded by an OSA (AQ6375, Yokogawa, Tokyo, Japan) with a sampling interval of 0.01 nm.

4. Results and Discussions

The obtained switchable output is shown in Fig. 4(a). At the beginning of the experiment, the SMF and the MMFBG were axially aligned. When the pump power was 2.03 W, an output spectrum with a lasing peak at 1973.51 nm was obtained. Then,

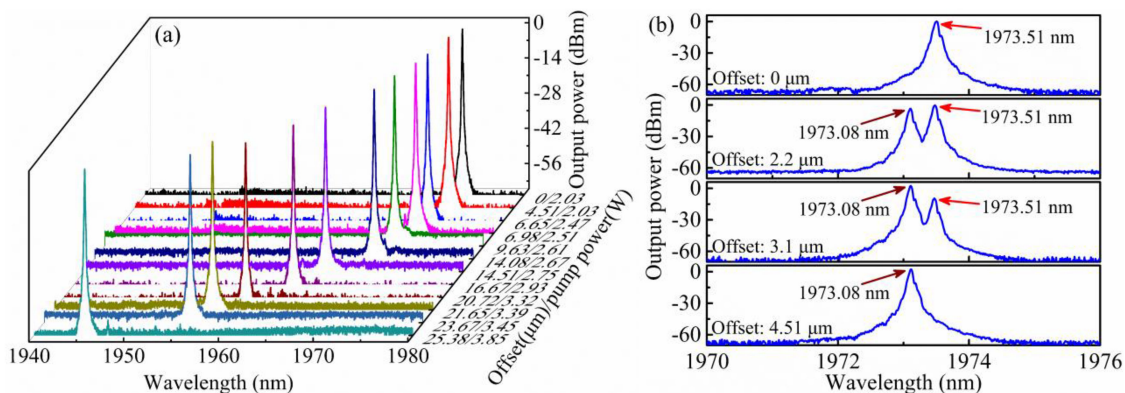


Fig. 4. (a) Switchable output of the TDFL, (b) detailed process of the switchable output.

the axial misalignment was applied to the SMF and MMFBG. When the axial misalignment (offset) was $4.51 \mu\text{m}$, the output spectrum obtained had a lasing peak at 1973.08 nm . With further increase of the axial misalignment, lasing output spectra could be obtained at shorter wavelength range. Due to the core mismatch of the SMF and MMFBG, the optical loss in the cavity increased, which led to the decreased output power when new laser lines were generated. Therefore, the pump power should be raised to ensure the continuous generation of new laser lines when the axial misalignment is increased. With an axial misalignment of $25.38 \mu\text{m}$ and a pump power of 3.85 W , the shortest output wavelength was obtained at 1945.35 nm . Further increasing the axial misalignment caused increased loss in the cavity and new laser lines could not be obtained even with a very high pump power.

The detailed process of the switchable output between the wavelength at 1973.51 and 1973.08 nm , shown in Fig. 4(b), reveals that, with the increase of the axial misalignment, the intensity at 1973.51 nm decreases and the intensity at 1973.08 nm increases gradually. Eventually, the output channel could be switched to a shorter wavelength region.

In theory, the separation between the lasing lines is almost a constant. However, in the experiment, the reflection peak of the MMFBG is not sharp enough as shown in Fig. 2(a), which leads to the reduction of the wavelength separation, because the lasing wavelengths within one reflection peak of the MMFBG could be obtained as shown in Fig. 4(b). In addition, when increasing the axial misalignment, some of the reflection peaks could not obtain enough gain and the output lasing lines locating at these wavelengths were not obtained, which increased the wavelength separation. Thus, the wavelength separation varied between different output wavelengths.

To demonstrate the stability of the laser, two of the output wavelengths at 1973.08 and 1971.94 nm were repeatedly scanned within one hour with a time interval of ten minutes. With an axial misalignment of $4.51 \mu\text{m}$ and a pump power of 2.03 W , an output wavelength at 1973.08 nm was obtained, as shown in Fig. 5(a), which also shows the repeated scans in the inset. The OSNR is higher than 65 dB , and the fluctuations of the center wavelength (f_λ) and output optical power (f_p) with respect to the observation time is shown in Fig. 5(b). The fluctuation of the center wavelength and optical power is less than 0.03 nm and 0.67 dB , respectively. When the axial misalignment and pump power is $6.65 \mu\text{m}$ and 2.47 W , respectively, the output spectrum has an OSNR higher than 65 dB , as shown in Fig. 5(c) with the repeated scans in the inset. The fluctuation of the center wavelength and output optical power are shown in Fig. 5(d) and are calculated to be less than 0.01 nm and 0.22 dB , respectively. The experimental results demonstrated that the proposed TDFL operated in a stable state. Notably, the optical fibers used in the experiment were glued on the stainless-steel plate with adhesive tape, which to some extent ensured the stable operation of the TDFL. According to the previous report [34], the variation of output wavelength with respect to the variation of temperature can be expressed as $\Delta\lambda_T = \lambda(\alpha + \xi)\Delta T$, where ΔT is the variation

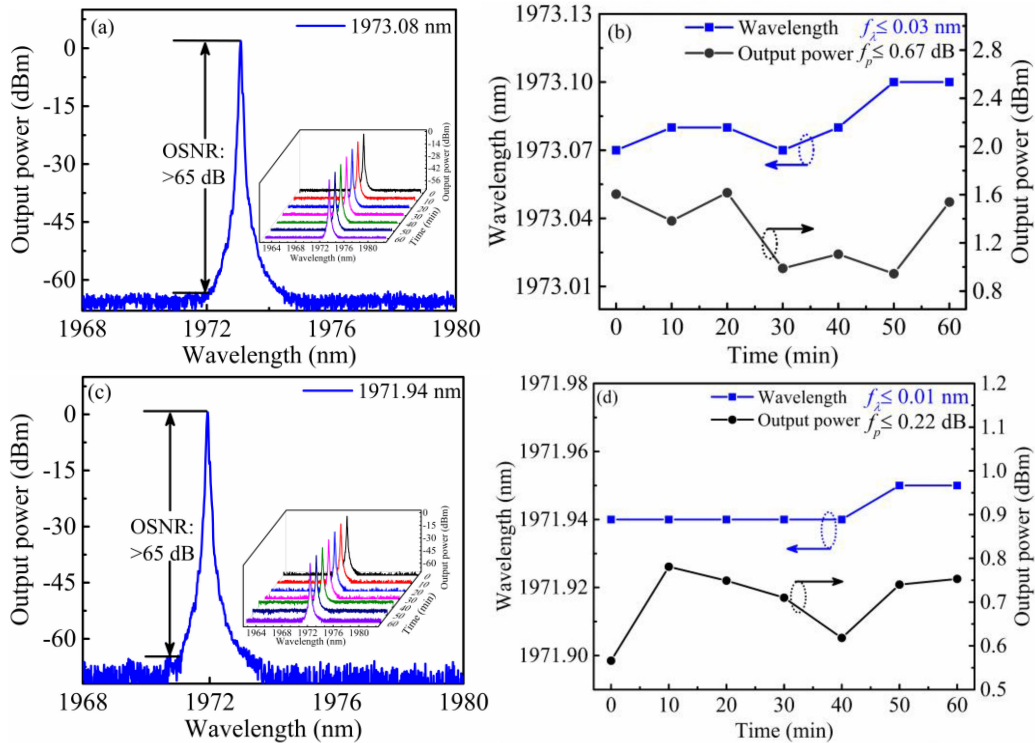


Fig. 5. Output spectrum peaks at (a) 1973.08 and (c) 1971.94 nm, output wavelength and power with respect to observation time at (b) 1973.08 and (d) 1971.94 nm.

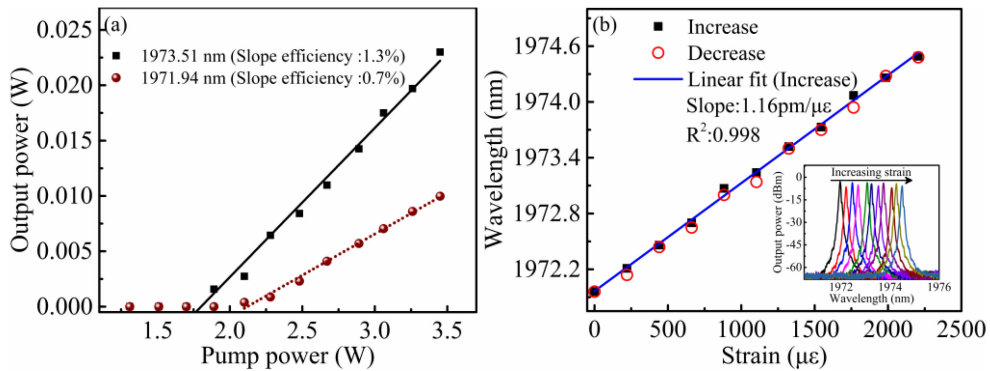


Fig. 6. (a) Slope efficiency of the proposed TDFL when the lasing wavelength is 1973.51 and 1971.94 nm, (b) variation of the output wavelength of the TDFL with respect to strain.

of temperature. α and ξ represents the thermal expansion coefficient and thermo-optic coefficient, respectively. Both the coefficients are positive number. Thus, with the increase of temperature, the output spectrum exhibits a red-shift. To further improve the stability, temperature control and vibration isolation should be implemented.

In addition, the output power was measured using a power meter (Ophir StarLite, Ophir-Spiricon, LLC., North Logan, UT, USA) when the output wavelength was at 1973.51 and 1971.94 nm, as shown in Fig. 6(a). The maximum slope efficiency was 1.3% at the output wavelength of 1973.51 nm. In this situation, the axial misalignment between the SMF and the MMFBG was 0. When the axial misalignment reached 4.51 μm , the slope efficiency at the lasing wavelength of

TABLE 1
Comparison of the Proposed TDFL with Previously Reported Switchable TDFLs Based on FBGs

Number of lasing lines	Maximum OSNR (dB)	Fluctuation of wavelength (nm)	Fluctuation of output power (dB)	Mechanism	Reference
6	59	0.02	0.71	PC	[14]
2	63	0.01	0.3	PC	[26]
6	<65	NA	NA	Gain and loss	[27]
2	<61	0.02	0.35	PC	[28]
12	>65	0.03	0.67	Axial misalignment	This work

1971.94 nm was 0.7%, which is almost half compared with that at the lasing wavelength of 1973.51 nm. The core mismatch between the SMF and MMFBG greatly influenced the slope efficiency. When the axial misalignment was further increased, the slope efficiency continuously decreased. Notably, the output power was not saturated in Fig. 6(a), indicating that the output power could be further improved by increasing the pump power. However, to protect the v-grooves, which were used to clamp the SMF and the MMFBG, of the fusion splicer, the pump power was not further increased.

Finally, the proposed TDFL was used as an optical fiber laser sensor to measure the strain. The MMFBG was clamped on the translation stages using fiber clamps. One of the stages was fixed and another one was movable. The initial wavelength was selected at 1971.94 nm, and the strain was applied on the MMFBG as the movable stage moved away from the fixed stage. The output spectrum was recorded once the strain was increased by $220.6 \mu\epsilon$ calculated by $\Delta L/L$, where ΔL (0.03 mm) is the distance moved by the movable stage, and L (13.6 cm) is the initial distance between the two translation stages. The output center wavelength was recorded both when the movable stage moved away from and towards the fixed stage, and the results are shown in Fig. 6(b). The inset in Fig. 6(b) shows the red-shift of the output spectrum with the increasing strain. For an FBG strain sensor, the variation of the output wavelength with respect to the variation of strain can be expressed as $\Delta\lambda = (1 - P_e)\lambda\Delta\epsilon$, where P_e is the effective elasto-optic coefficient, which is smaller than 1 [35]. Thus, the output spectrum shows a red-shift. The sensitivity of the optical fiber laser sensor is $1.16 \text{ pm}/\mu\epsilon$ and the goodness of fit is 0.998. Remarkably, the proposed fiber laser sensor is better than those in previous reports using FBGs with respect to the sensitivity [31], [34], [36]. The possible reason may lie in that the sensitivity $(1 - P_e)\lambda$ is related to the specified lasing wavelength. Considering the effective elasto-optic coefficient a constant, when a longer wavelength was selected, a higher sensitivity could be obtained.

The proposed fiber laser is compared with some of the previously reported TDFLs with switchable single wavelength output using FBG, as shown in Table 1. The number of lasing lines in the TDFL proposed in this article is 12, which is more than in those reported [14], [26]–[28], and the maximum OSNR is obtained. The fluctuation of the output wavelength is higher than that in the previous reports [14], [26], [28], and a moderate fluctuation of output power is obtained. In addition, compared with introducing the axial misalignment to achieve the switchable output, adjusting the PC is always random and inaccurate [14], [26], [28], balancing the gain and loss in the cavity would complicate the system as 10 tubular mounts should be incorporated [27]. Overall, the proposed TDFL has the advantages of having a large number of switchable output wavelengths and a high OSNR, as well as being more accurately controlled.

5. Conclusion

In summary, a twelve-wavelength switchable TDFL was proposed and demonstrated. A polarization independent MMFBG with multireflection peaks was selected to serve as an in-line all fiber filter. The reflection spectrum of the MMFBG was studied under different launching conditions using a commercially available fusion splicer. Based on the analyses, the TDFL was constructed with an OSNR higher than 65 dB. The maximum fluctuation of the center wavelength and output power was less than 0.03 nm and 0.67 dB, respectively, as monitored by an OSA with a sampling interval of 0.01 nm within an hour. The maximum slope efficiency was 1.3%, and thus needs to be further improved in future work. In addition, the proposed fiber laser was used as an optical fiber laser sensor to measure the strain. A sensitivity of $1.16 \text{ pm}/\mu\epsilon$ was obtained, which is higher than that obtained by the reported FBG-based optical fiber sensors in the $1.5 \mu\text{m}$ band, and a likely reason is explained. The proposed fiber laser may find useful application in optical fiber laser sensors and free space optical communication systems.

References

- [1] E. Chen, S. Liu, P. Lu, J. Zhang, and Z. Lian, "Tunable $2 \mu\text{m}$ fiber laser utilizing a modified sagnac filter incorporating cascaded polarization maintaining fibers," *IEEE Photon J.*, vol. 12, no. 1, Feb. 2020, Art. no. 1500507.
- [2] K. Xu *et al.*, "High speed single-wavelength modulation and transmission at $2 \mu\text{m}$ under bandwidth-constrained condition," *Opt. Exp.*, vol. 25, no. 4, pp. 4528–4534, Feb. 2017.
- [3] M. U. Sadiq *et al.*, "40 Gb/s WDM transmission over 1.15-km HC-PBGF using an in-p-based Mach-Zehnder modulator at $2 \mu\text{m}$," *J. Lightw. Technol.*, vol. 34, no. 8, pp. 1706–1711, Apr. 2016.
- [4] P. Lin, T. Wang, W. Ma, J. Chen, Z. Jiang, and C. Yu, " $2\text{-}\mu\text{m}$ free-space data transmission based on an actively mode-locked holmium-doped fiber laser," *IEEE Photon. Technol. Lett.*, vol. 32, no. 5, pp. 223–226, Mar. 2020.
- [5] F. J. McAleavy, J. O'Gorman, J. F. Donegan, B. D. MacCraith, J. Hegarty, and G. Maze, "Narrow linewidth, tunable tm^{3+} -doped fluoride fiber laser for optical-based hydrocarbon gas sensing," *J. Sel. Topics Quantum Electron.*, vol. 3, no. 4, pp. 1103–1111, Aug. 1997.
- [6] A. Ghosh, A. S. Roy, S. D. Chowdhury, R. Sen, and A. Pal, "All-fiber tunable ring laser source near $2 \mu\text{m}$ designed for CO_2 sensing," *Sensors Actuators B Chem.*, vol. 235, pp. 547–553, 2016.
- [7] M. Michalska *et al.*, "Highly stable, efficient Tm-doped fiber laser—A potential scalpel for low invasive surgery," *Laser. Phys. Lett.*, vol. 13, no. 11, Sep. 2016, Art no.115101.
- [8] O. Traxer and E. X. Keller, "Thulium fiber laser: The new player for kidney stone treatment? A comparison with holmium: YAG laser," *World. J. Urol.*, vol. 38, pp. 1883–1894, 2019.
- [9] H. Kalaycıoğlu, P. Elahi, Ö. Akçaalan, and F. Ö. İlday, "High-repetition-rate ultrafast fiber lasers for material processing," *J. Sel. Topics Quantum Electron.*, vol. 24, no. 3, pp. 1–12, May/Jun. 2018.
- [10] J. Geng, Q. Wang, Y. Lee, and S. Jiang, "Development of eye-safe fiber lasers near $2 \mu\text{m}$," *J. Sel. Topics Quantum Electron.*, vol. 20, no. 5, pp. 150–160, Sep/Oct. 2014.
- [11] I. Kubat *et al.*, "Thulium pumped mid-infrared $0.9\text{--}9\mu\text{m}$ supercontinuum generation in concatenated fluoride and chalcogenide glass fibers," *Opt. Exp.*, vol. 22, no. 4, pp. 3959–3967, Feb. 2014.
- [12] X. Ma *et al.*, "Widely tunable thulium-doped fiber laser based on multimode interference with a large no-core fiber," *J. Lightw. Technol.*, vol. 32, no. 19, pp. 3234–3238, Oct. 2014.
- [13] Y. Guo *et al.*, "Stable multi-wavelength thulium-doped fiber laser with two cascaded single-mode-four-mode-single-mode fiber interferometers," *IEEE Access*, vol. 9, pp. 1197–1204, 2021.
- [14] L. Zhang *et al.*, "Six-wavelength-switchable narrow-linewidth thulium-doped fiber laser with polarization-maintaining sampled fiber Bragg grating," *Opt. Laser. Technol.*, vol. 136, Jan. 2021, Art. no. 106788.
- [15] Q. Zhang *et al.*, "5 W ultra-low-noise $2 \mu\text{m}$ single-frequency fiber laser for next-generation gravitational wave detectors," *Opt. Lett.*, vol. 45, no. 17, pp. 4911–4914, Sep. 2020.
- [16] V. Voropaev *et al.*, "Generation of multi-solitons and noise-like pulses in a high-powered thulium-doped all-fiber ring oscillator," *Sci. Rep.*, vol. 9, no. 1, pp. 1–11, Dec. 2019, Art. no. 18369.
- [17] H. Li *et al.*, "Generation of switchable multiwavelength solitons with wide wavelength spacing at $2 \mu\text{m}$," *Opt. Lett.*, vol. 44, no. 10, pp. 2442–2445, May. 2019.
- [18] X. Guan *et al.*, "55 W kilohertz-linewidth core-and in-band-pumped linearly polarized single-frequency fiber laser at 1950 nm ," *Opt. Lett.*, vol. 45, no. 8, pp. 2343–2346, Apr. 2020.
- [19] E. H. Escobar *et al.*, "Experimental study of an in-fiber acousto-optic tunable bandpass filter for single-and dual-wavelength operation in a thulium-doped fiber laser," *Opt. Exp.*, vol. 27, no. 26, pp. 38602–38613, Dec. 2019.
- [20] X. Chen *et al.*, "Wavelength-flexible thulium-doped fiber laser based on digital micromirror array," *Micromachines.*, vol. 11, no. 12, 2020, Art. no. 1036.
- [21] A. Camarillo-Avilés *et al.*, "Stable multi-wavelength thulium-doped all-fiber laser incorporating a multi-cavity Fabry–Perot filter," *IEEE Photon. J.*, vol. 11, no. 6, Dec. 2019, Art. no. 7105307.
- [22] B. Posada-Ramírez *et al.*, "Study of a hi-bi FOLM for tunable and dual-wavelength operation of a thulium-doped fiber laser," *Opt. Exp.*, vol. 25, no. 3, pp. 2560–2568, Feb. 2017.
- [23] P. Zhang *et al.*, "Stable multi-wavelength thulium-doped fiber laser based on all-fiber Mach-Zehnder interferometer," *Chin. Opt. Lett.*, vol. 12, no. 11, Nov. 2014, Art. no. 111403.

- [24] Q. Qin *et al.*, "Stable, precisely controlled, and switchable thulium-doped fiber laser based on cascaded mode interference filters," *Opt. Exp.*, vol. 29, no. 7, pp. 9786–9796, Mar. 2021.
- [25] B. Ibarra-Escamilla *et al.*, "Abrupt-tapered fiber filter arrangement for a switchable multi-wavelength and tunable Tm-doped fiber laser," *Opt. Exp.*, vol. 26, no. 12, pp. 14894–14904, Jun. 2021.
- [26] W. Peng *et al.*, "1.94 μm switchable dual-wavelength Tm³⁺ fiber laser employing high-birefringence fiber Bragg grating," *Appl. Opt.*, vol. 52, no. 19, pp. 4601–4607, Jul. 2013.
- [27] J. Li *et al.*, "Wide wavelength selectable all-fiber thulium doped fiber laser between 1925 nm and 2200 nm," *Opt. Exp.*, vol. 22, no. 5, pp. 5387–5399, Mar. 2014.
- [28] S. Liu *et al.*, "Switchable single-polarization dual-wavelength TDFL using PM Fabry–Perot filter," *Opt. Fiber. Technol.*, vol. 29, pp. 1–5, May. 2016.
- [29] M. Ding *et al.*, "High-sensitivity thermometer based on singlemode-multimode FBG-singlemode fiber," *Opt. Laser. Technol.*, vol. 96, pp. 313–317, Nov. 2017.
- [30] T. Yang *et al.*, "Fiber Bragg gratings inscriptions in multimode fiber using 800 nm femtosecond laser for high-temperature strain measurement," *Opt. Laser. Technol.*, vol. 93, pp. 138–142, Aug. 2017.
- [31] Q. Wang *et al.*, "Fiber Bragg grating with a waveguide fabricated in no-core fiber and multimode fiber," *Opt. Lett.*, vol. 44, no. 11, pp. 2693–2696, Jun. 2019.
- [32] C. Lu *et al.*, "Fiber Bragg grating spectra in multimode optical fibers," *J. Lightw. Technol.*, vol. 24, no. 1, pp. 598–604, Jan. 2006.
- [33] T. Mizunami *et al.*, "Bragg gratings in multimode and few-mode optical fibers," *J. Lightw. Technol.*, vol. 18, no. 2, pp. 230–235, Feb. 2000.
- [34] W. Zhao and R. O. Claus, "Optical fiber grating sensors in multimode fibers," *Smart. Mater. Struct.*, vol. 9, pp. 212–214, Apr. 2000.
- [35] E. Li, "Sensitivity-enhanced fiber-optic strain sensor based on interference of higher order modes in circular fibers," *IEEE Photon. Technol. Lett.*, vol. 19, no. 16, pp. 1266–1268, Aug. 2007.
- [36] X. Gao *et al.*, "A dual-parameter fiber sensor based on few-mode fiber and fiber Bragg grating for strain and temperature sensing," *Opt. Commun.*, vol. 454, Jan. 2011, Art. no. 124441.